Received: 20 December 2020 | Revised: 21 February 2021 | Accepted: 23 February 2021

IET Smart Grid

DOI: 10.1049/stg2.12036

The Institution of Engineering and Technology WILEY

ORIGINAL RESEARCH PAPER

Optimisation, benchmark testing and comparison of droop control variants in microgrids

Simon Eberlein | **Krzysztof Rudion**

Department of Power Transmission and High Voltage Technology, University of Stuttgart, Pfaffenwaldring, Stuttgart, Germany

Correspondence

Simon Eberlein, Department of Power Transmission and High Voltage Technology, University of Stuttgart, Pfaffenwaldring 47, 70569, Stuttgart, Germany.
Email: simon.eberlein@ieh.uni-stuttgart.de

Funding information

Open Access funding enabled and organized by Projekt DEAL

Abstract

Grid-forming inverter control is recently discussed for bulk power systems and is already in use for islanded microgrids. A common control type is the droop control. Numerous variants of the basic droop control have been proposed. However, there is lack of performance comparison of the droop variants in literature. Their superiority has only been demonstrated for some specific microgrid scenarios. This work composes benchmark scenarios to assess and compare the applicability of droop control variants and also their combination with virtual impedances under practical conditions. A number of microgrid topologies and the interaction with synchronous machines are considered to benchmark the performance. Static criteria, such as the steady-state power sharing, as well as dynamic stability criteria, are taken into account for modal analysis. To guarantee a meaningful comparison, a genetic algorithm tailored to the problem is used to optimise controller parameters for each controller type. Results indicate that the combination with virtual impedance has a more decisive effect on stability than the droop variant. The outcome is relevant for microgrid stability analysis in numerous contexts, such as optimal placement of inverters or topology optimisation, where the choice of the most suitable controller type with optimised parameter sets is key.

1 | INTRODUCTION

The benefits of microgrids range from economic and technical to environmental and social benefits [1]. Coordinated active and reactive power curtailment, reduced losses and enhanced reliability due to islanding capability are among the technical benefits. Key aspects of the islanded operation of microgrids are power sharing among distributed energy resources (DER) and small-signal stability.

Numerous control strategies have been proposed in literature for the power sharing in microgrids, which are also referred to as primary control strategies. Reviews are given in [2, 3]. One of the most widely used control strategies is the droop control and its variants, which emulate the dynamics of synchronous machines to some extent and do not fall back on communication.

One shortcoming of the conventional droop control is that it is based on the assumption that the lines are predominantly inductive, which does not apply to low-voltage microgrids. However, the grid-side filter inductance favourably decreases the R/X-ratio. Other disadvantages are that frequency and voltage deviate from their nominal values at steady-state and that there is an inherent trade-off between load sharing accuracy and frequency and voltage regulation [4]. In addition, the voltage drop over the line impedances deteriorates the accuracy of the reactive power sharing, which can cause large circulating currents [5, 6].

A large number of variations of the conventional droop control have been proposed in literature to enhance the performance [3]. One possibility is to add a transient term, which is the derivative of the power measurement. The superiority of the transient droop over the conventional droop is shown for a small microgrid with fixed parameters (i.e. line length, R/X ratio) and without parameter optimisation (i.e. optimisation of static droop gains etc.) in [7]. The interaction with virtual impedance is not investigated.

Another approach is to add a feed-forward gain that stabilises the frequency droop. It has been used since the early stages of droop-based inverter control [8].

To overcome the issue of large line R/X-ratio, the virtual frame transformation is proposed in [9]. In this way, the frequency and voltage control are decoupled, assuming that the exact angle of the line impedance is known. The practicability of the approach for the parallel operation of inverters is exemplified in a small test system with very large impedances connecting the inverters, but not under practical microgrid conditions. The performance is neither compared to the conventional droop control nor to any other droop variant.

The angle of the line impedances is usually not known, as it also depends on the present load in a microgrid. To tackle this problem, [10] proposes a fixed angle of 45° for the frame transformation, which was derived based on system stability optimisation under various conditions. The applicability is demonstrated in a small test system with large line impedances and the superiority over the conventional droop control is shown for this distinct case. The selected low-pass filter time constant of the droop control is very large, leading to settling times of up to 1 s. Combination of the droop variant with virtual impedance is not considered.

Network impedance estimation for frame transformation is conducted in [5]. Virtual frame transformation is also applied in [11] and an alternative virtual frequency-voltage frame transformation is proposed in [12].

Furthermore, an inverse droop control, where the frequency depends on the active power and the voltage magnitude depends on the reactive power is suggested in [13, 14]. This is equivalent to the virtual frame transformation using an angle of 90°. However, the inverse droop is not compatible with the inherent coupling between the frequency and active power of synchronous machines (SMs), which is a consequence of the rotating inertia.

In [15] it is proposed to use the virtual flux instead of the inverter output voltage in the droop equations. Voltage angle droop is utilised in [16] instead of frequency droop. However, it necessitates low-bandwidth communication. Further approaches apply a quadratic or other non-linear function in the droop equations [17–19].Virtual impedance (VI) can be used to emulate the voltage drop over a line impedance [9, 20]. In this way, the controller stability is enhanced due to the adjustable R/X-ratio. Moreover, better reactive power sharing can be obtained and the damping of parallel inverters is increased [6].

Besides the choice of the power sharing strategy, the tuning of the control parameters has a crucial impact on the performance. The optimisation of control parameters can be classified into offline and online tuning, where parameters are either tuned beforehand or during operation, respectively. This work focuses on offline tuning.

Droop controlled DER are optimised in a small microgrid in [21] utilising particle swarm optimization (PSO). The criteria for the fitness function are the harmonic distortion and the area criterion for power sharing. Non-linear droop is optimised with respect to power sharing and cost reduction in [19] also using PSO. The optimal value of an algebraic type VI is derived in [22]. A number of criteria, such as voltage boundaries and reactive power sharing, are incorporated using weighting factors. Differential evolution is used for the optimisation of inverters with VI in [20]. In [23], first the feasible range of controller parameters is detected with modal analysis. Then the area criterion is used to optimise the power sharing with a genetic algorithm (GA).

In the first part of the review above it was shown that numerous droop variants have been proposed in literature. Most works demonstrate improvements in comparison to the conventional droop control only or simply exemplify the applicability for one specific test case. There is clearly a lack of performance comparison between the droop variants. Furthermore, it is hardly investigated how the droop variants perform in combination with VI.

It was shown in the second part of the review that heuristic methods, such PSO or GA, are used for the parameter tuning, as this is a complex optimisation problem which can hardly be solved analytically. A simple scenario is usually considered, where either the interaction between droop controlled inverters or between inverters and SMs are investigated. The line length and the R/X-ratio are assumed to be fixed parameters. The number of control parameters incorporated in the optimisation is normally limited to the most influential parameters, such as the droop coefficients. Other relevant parameters, like the PI-controller of the governor (GOV) of SMs, are not considered.

Research on the stability of microgrids in many contexts, such as the placement of DER [24] or microgrid reconfiguration [25], relies on the usage of optimised controllers and parameter sets to ensure that results are meaningful. However, at the moment researchers and practitioners are faced with the task of choosing from a large number of possible controller designs without being able to classify their advantages and disadvantages. Hence, the necessity for the optimisation and comparison of droop variants is obvious and is carried out in this work. The goal is to optimise, test and compare the performance of droop variants in several benchmark scenarios to be able to make a statement or recommendation on their applicability and additionally provide optimised parameter sets. Due to the large number of droop variants, only a limited selection can be investigated and we focussed on three of the most popular ones: The transient droop (TD), feed-forward droop (FFD) and virtual frame transformation droop (FTD). Some similarities between the variants are pointed out.

Influential controller parameters of the compared droop variants are optimised to allow for a fair assessment. To handle the complexity of the optimisation problem, artificial intelligence which is a GA, is applied. The proposed GA is tailored to this computational intensive optimisation problem.

Benchmark scenarios are designed to allow for the comparison of control strategies under various microgrid scenarios to assess the controllers under practical conditions. This differs from previous publications, where the practicability was shown only for a very limited number of special cases. Dynamic stability criteria, such as eigenvalues, as well as static criteria, such as steady-state power sharing, are considered.

The main contributions of this work are:

- Select some of the most popular droop variants and describe differences and similarities.

- Use a GA tailored to the problem to optimise the controller parameters, including VI, to allow for a fair comparison of the droop variants.
- Evaluate the droop variants using benchmark tests and provide guidance for their practicability as well as optimised parameter sets.

The rest of this work is organised as follows: The model of the microgrid and its components is introduced in Section 2. The Benchmark tests are elaborated in Section 3 and the GA is described in Section 4. Section 5 shows the results and a conclusion is given in Section 6.

2 | MODELLING

2.1 | Inverter

The model of a three-phase droop controlled inverter with *LCL*-filter (single line diagram) and a VI are illustrated in Figure 1 [26]. The modelling approach from [27] is used, which has been extensively referred to in literature and validated by experiment. The model also comprises a VI. The power electronic converter is simplified by the averaged switching model [28].

The model includes the inner loops of the voltage and current controller, which are implemented as PI-controllers (see Figure 2 with the proportional gains $k_{p,v}/k_{p,c}$ and integral gains $k_{i,v}/k_{i,c}$, respectively). Furthermore, the inner loops contain the feed-forward gains FF_v and FF_c to enhance the stability [26]. Pole cancellation is used so that the closed loop transfer function of the current controller approximates a first order lag. The tuning of the voltage controller considers the limitation of harmonic propagation. Parameters are given in the Appendix [26].

2.2 | Diesel synchronous generator

Figure 3 depicts the diesel genset model from [29] used in this work. The electrical part of the SM is represented by a sixth order model and the mechanical part is represented by the second order swing equation [30]. Droop control is used, for maximum flexibility, the FTD (see Section 2.3) and a VI are implemented. Due to the larger time constants of SMs, the TD and FFD are only suitable for inverters as they influence the response at fast time scales. FTD on the other hand also takes effect on slower mechanisms and the static power sharing. The latter also applies to the VI. Hence, FTD and VI are compatible with SMs and enhance their flexibility and are applied in all scenarios with SMs in this work.

The AC5A model depicted in Figure 4 with brushless exciter and a PI-controller is used for the automatic voltage regulator (AVR). It consists of a main regulator and an exciter with saturation. It is widely used by the industry, especially for small size gensets [31, 32].

The GOV is illustrated in Figure 5. It consists of a PI-controller, current driver, actuator and the engine, represented by a dead time element [31, 32]. Parameters are given in the Appendix.

2.3 | Droop control

2.3.1 | Conventional droop control

Active power P_L and reactive power Q_L transmission over a line with the impedance $\underline{Z}_L = Ze^{j\gamma} = R_L + jX_L$ can be described as [9].

$$P_L = \frac{V_1}{R_L^2 + X_L^2}[R_L(V_1V_2cos\delta) + XV_2sin\delta], \quad (1)$$

$$Q_L = \frac{V_1}{R_L^2 + X_L^2}[-R_LV_2sin\delta + X_L(V_1 - V_2cos\delta)], \quad (2)$$

where V_1 and V_2 are the voltages at the line terminals and δ is the angular difference. Assuming a small δ and a predominantly inductive line, this can be simplified to

$$\delta \cong \frac{X_LP_L}{V_1V_2}, \quad (3)$$

$$V_1 - V_2 \cong \frac{X_LQ_L}{V_1}. \quad (4)$$

The relations between δ and active power and the voltage magnitude difference and reactive power are exploited by the conventional droop control, which are done based on the following control principle [33]:

$$\omega_{droop} = \omega_0 - m_\omega(p_{LPF} - p_0), \quad (5)$$

$$v_{droop} = v_0 - m_v(q_{LPF} - q_0). \quad (6)$$

The frequency ω_{droop} and voltage amplitude v_{droop} are controlled according to the low-pass filtered active power p_{LPF} and reactive power q_{LPF}, depending on the droop coefficients m_ω and m_v. A first order low-pass filter with the cut-off frequency ω_c is used in the power calculation block. Further insight into the selection of the cut-off frequency is given in [7, 26]. Parameters ω_0 and v_0 are usually set to their nominal values (1 pu). p_0 and q_0 provide degrees of freedom and may be set by the secondary controller. They are set to zero in this work. The angle θ is attained by integrating ω_{droop}.

2.3.2 | Transient droop control

Combining the conventional static droop with a transient term was first proposed in [7]:

$$\omega_{droop} = \omega_0 - m_\omega(p_{LPF} - p_0) - m_{\omega,t}sp_{mea}, \quad (7)$$

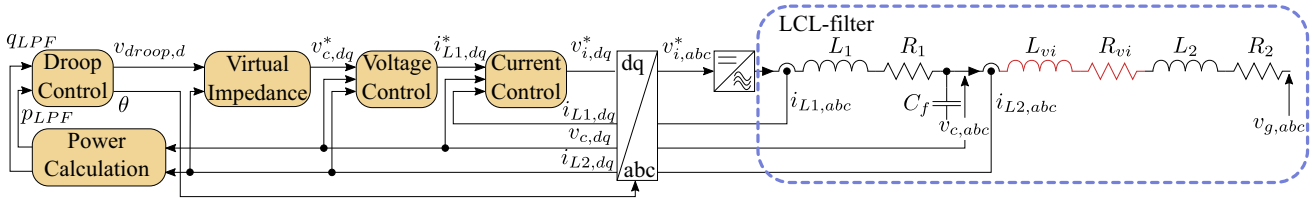

FIGURE 1 Overview of grid-forming droop controlled inverter with LCL-filter

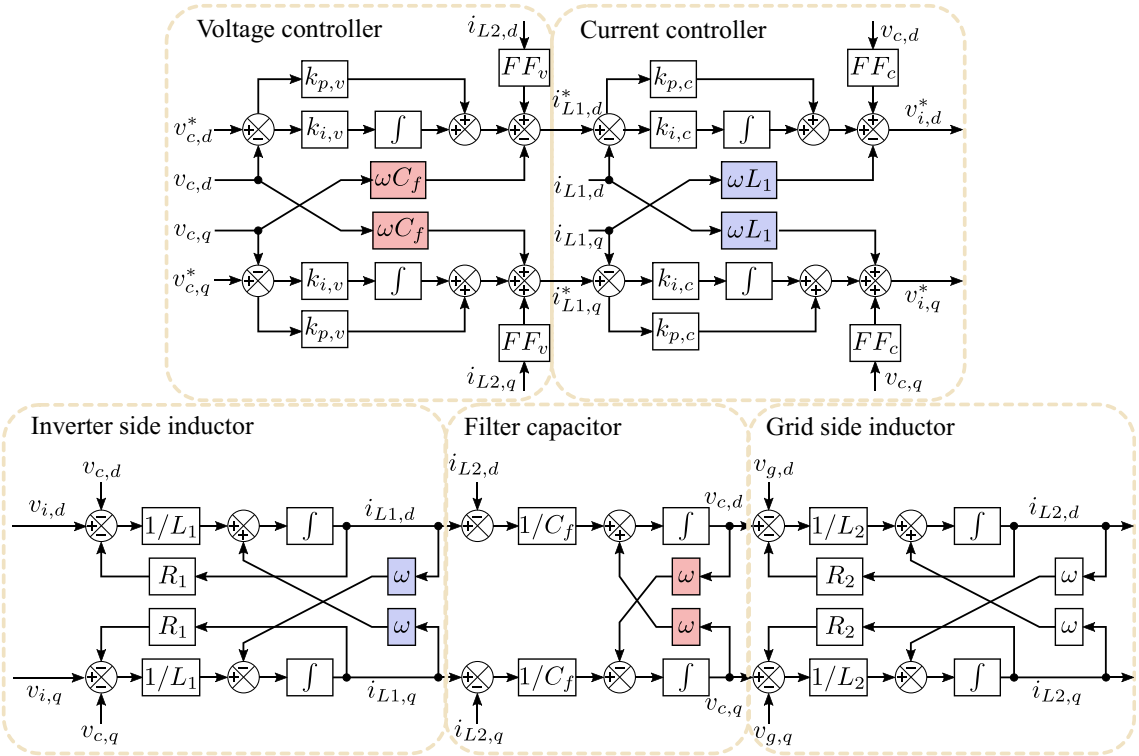

FIGURE 2 Voltage and current controllers and LCL-filter of grid-forming inverter in the *dq*-reference frame

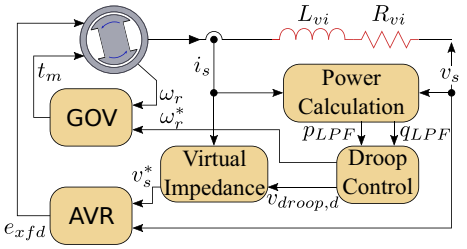

FIGURE 3 Overview of grid-forming droop controlled synchronous machine

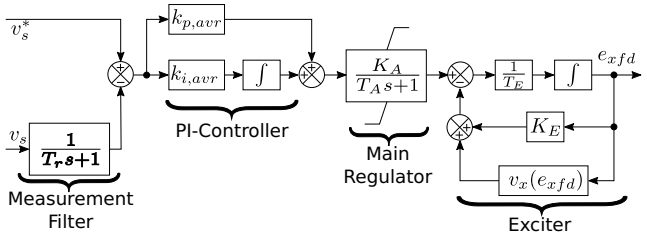

FIGURE 4 AVR of the diesel genset

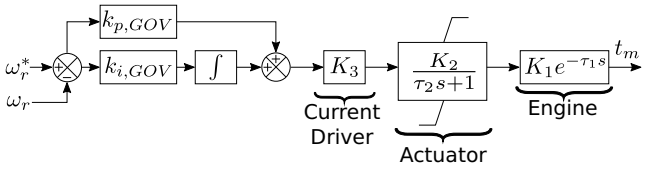

FIGURE 5 GOV of the diesel genset

$$v_{droop} = v_0 - m_v(q_{LPF} - q_0) - m_{v,t} s q_{mea}, \tag{8}$$

where p_{mea} and q_{mea} are the measured active and reactive power and $m_{\omega,t}$ and $m_{v,t}$ are the active and reactive power transient droop coefficients, respectively, and s is the Laplace operator. A high-pass filter is usually employed in practice instead of a pure derivative term. The same cut-off frequency

as for the low-pass filter is also used for the high-pass filter in this work [7, 26].

In [7], advantages of the transient droop over the conventional droop are demonstrated. It preserves the dynamics and stability at different loading conditions. However, only a small microgrid with fixed parameters (i.e. line length, R/X ratio) is used for demonstration. Combination with VI is not considered.

2.3.3 | Active power feed-forward

The control in Figure 6 is similar to the conventional frequency droop control, except for the feed-forward gain $m_{\omega,ff}$ [8]. Its purpose is the stabilisation of the frequency droop. The angle θ of the droop control can be written as follows, depending on the filtered active power p_{LPF} :

$$\theta = \frac{1}{s}(\omega_0 - m_\omega(p_{LPF} - p_0)) - m_{\omega,ff}p_{LPF}, \tag{9}$$

To compare active power feed-forward and transient droop, (7) is integrated to arrive at the angle of the droop control:

$$\theta = \frac{1}{s}(\omega_0 - m_\omega(p_{LPF} - p_0) - m_{\omega,t}sp_{mea}), \tag{10}$$

If the cut-off frequency of the high-pass filter of the transient droop is the same as for the low-pass filter in the feed-forward approach ($sp_{mea} \approx \frac{s\omega_c p_{mea}}{s+\omega_c} = sp_{LPF}$), (10) is brought to the form:

$$\theta = \frac{1}{s}(\omega_0 - m_\omega(p_{LPF} - p_0)) - m_{\omega,t}p_{LPF}. \tag{11}$$

If $m_{\omega,t} = m_{\omega,ff}$, (11) is equal to (9) and the frequency droop control is similar in both approaches. The advantage of the feed-forward droop is that no high-pass filter is necessary, which can cause problems when harmonics are present.

2.3.4 | Virtual frame transformation

Modified active power P' and reactive power Q' are used in the virtual frame transformation [9]. An orthogonal linear rotational transformation matrix T_{VF} is applied, which depends on the line impedance $Ze^{j\gamma}$:

$$\begin{bmatrix} P' \\ Q' \end{bmatrix} = T_{VF}\begin{bmatrix} P \\ Q \end{bmatrix} = \begin{bmatrix} sin(\gamma) & -cos(\gamma) \\ cos(\gamma) & sin(\gamma) \end{bmatrix}\begin{bmatrix} P \\ Q \end{bmatrix} = \begin{bmatrix} X_L/Z_L & -R_L/Z_L \\ R_L/Z_L & X_L/Z_L \end{bmatrix}\begin{bmatrix} P \\ Q \end{bmatrix} \tag{12}$$

Applying this transformation to the line power transmission in (1) and (2) finally results in [9]:

$$sin(\delta) = \frac{Z_L P'_L}{V_1 V_2} \tag{13}$$

$$V_1 - V_2 cos(\delta) = \frac{Z_L Q'_L}{V_1}. \tag{14}$$

Assuming a small δ and small voltage difference $V_1 - V_2$, the angle is related only to P', and the voltage difference only to Q'. A small test system with very large impedances connecting parallel inverters is used in [9] to show the practicability of the approach. However, the applicability under practical microgrid conditions is not demonstrated. Furthermore, there is no comparison of the performance to the conventional droop control or any other droop variant. A thorough parameter optimisation is not conducted.

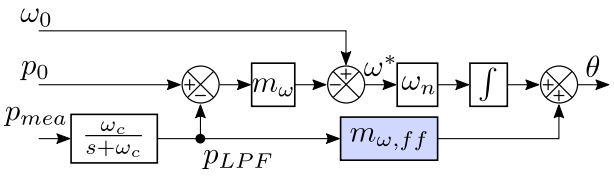

FIGURE 6 Droop control with feed-forward

2.4 | Virtual impedance

The algebraic type VI $\underline{z}_{vi} = r_{vi} + j\omega l_{vi}$ (in per unit) emulates a voltage drop $\Delta\underline{v}_{vi}$ depending on the grid-side inductance current $\underline{i}_{L2}$:

$$\Delta\underline{v}_{vi} = \underline{i}_{L2}\underline{z}_{vi} = \underline{i}_{L2}(r_{vi} + j\omega l_{vi}). \tag{15}$$

$\Delta\underline{v}_{vi}$ is subtracted from the droop voltage $v_{droop}e^{j\theta}$. The realisation in the inverter control scheme is shown in Figure 1. It is also shown in Figure 1 that the effect of VI is to add to the grid-side impedance of the LCL filter. For the SM, the stator current is used instead of the grid-side inductor current $\underline{i}_{L2}$. The realisation in the control scheme and the effect of the VI are depicted in Figure 3.

Some advantages of VI are enhanced stability due to the adjustable R/X ratio, improved damping especially when line impedance between inverters is low and better reactive power sharing at steady-state [6, 26]. On the other hand, the increased voltage drop over the VI may violate the voltage constraints of the network.

2.5 | Loads

This work focuses on the dynamic interactions of DER. Hence, a simple load model is implemented. As elaborated in

Section 3.3, the DER controllers are assessed according to their response to load fluctuations. To allow for a fair comparison of the controllers, it must be ensured that load steps in the network are independent from the DER controllers. For example, the voltage magnitude in the network can be dependent on the DER controller. If the loads are voltage dependent, like for example constant impedance loads, the impact of switching of loads varies depending in the DER controller. DER controllers that lead to low voltage levels would have an undesired advantage, because the disruption of load switching is lower (smaller active and reactive power change) and easier to handle by the DER controller. Therefore, the optimisation algorithm would prefer controllers that cause low voltage levels. However, low voltage levels are not the actual goal of the optimisation.

Instead, a constant active and reactive power current source model is used that is independent from DER controllers or controller parameters. The supplied current is given as:

$$i^*_{Load,d} = \frac{2}{3}\frac{p^* v_{POC,d} + q^* v_{POC,q}}{v^2_{POC,d} + v^2_{POC,q}}, \tag{16}$$

$$i^*_{Load,q} = \frac{2}{3}\frac{p^* v_{POC,q} - q^* v_{POC,d}}{v^2_{POC,d} + v^2_{POC,q}}, \tag{17}$$

where v_{POC} is the voltage at the point of coupling. A low pass filter with a time constant of 5 ms is used for the current $i^*_{Load,dq}$ to avoid the algebraic loop.

2.6 | Microgrid

Benchmark models have been used for a long time to assess and compare the performance of controllers in power system research [34] and there exist also generic benchmark systems for low voltage (LV) microgrids [35]. However, to the authors' knowledge, no agreed benchmark system with a clear focus on microgrid stability exists.

The benchmark system should be of small and simple structure. This reduces the computational cost of the numerous simulations that must be run in heuristic parameter optimisation. Moreover, a simple structure facilitates the correlation of controller performance with certain properties of the microgrid, such as the R/X ratio of lines or their length. These correlations cannot be represented uniquely in a more complex topology with various line lengths and R/X ratios. Furthermore, the simple topology lends itself to simulate worst-case scenarios with either very short or very long lines. In addition, the switching of one load is more disruptive compared to larger systems with a number of relatively small loads. This further challenges the DER control.

The LV microgrid depicted in Figure 7 is used for the optimisation and benchmark testing of the droop control variants in this work. It comprises a line and two nodes, each connecting one DER and one load. It incorporates the main

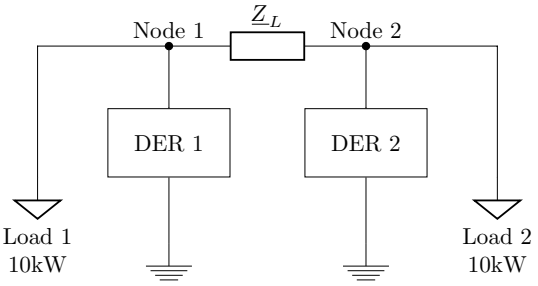

FIGURE 7 Microgrid with two nodes

dynamic characteristics of more complicated microgrids, despite its simple structure [23, 36, 37]. The line is modelled in the $dq0$ reference frame as a system of differential equations [38]. Microgrid parameters are varied to accommodate for more complex topologies, which is elaborated in Section 3.1.

3 | BENCHMARK TESTS

3.1 | Scenarios

Various cases are investigated, representing the conditions to which DER are exposed in LV microgrids. The DER at both nodes of the microgrid can either be two power electronic devices (PED) or one PED and one diesel SM, allowing for the analysis of the interaction between the types. The line length is either 30 or 400 m. Short lines and low impedance between DER challenge the stability [24, 25], whereas long lines impair the steady-state power sharing due to the larger voltage drop. The R/X-ratio of the line affects the droop control, as was shown in Section 2.3.1, and is either set to 3.9 or 7.7, which represents the typical range for LV networks.

For the benchmark scenarios, line length and R/X-ratios are varied, resulting in four cases/combinations. These four cases are tested for a microgrid with two PED and one PED and one SM. Moreover, in the benchmark scenario called 'all cases', the two DER combinations are combined, that is, parameters are optimised for the case of two PED as well as the combination of PED and SM. Varying line length and R/X-ratio, this sums up to eight cases. Hence, the parameter set from the 'all cases' benchmark scenario is suitable for a large variety of microgrid applications.

The response to active/reactive power load fluctuations is a crucial characteristic of primary control. The loads of the microgrid are varied every 5 s in time-domain simulations to analyse several load configurations. On one hand, this allows to investigate the transient response. On the other hand, the static constraints described in Section 3.2 are evaluated for these load cases. Load 1 is initially on, whereas load 2 is off. At t = 5 s, load 2 is turned on. At t = 10 s, the reactive power of load 1 is turned off. At t = 15, the active power of load 1 is turned off. At t = 20 s, the reactive power of load 2 is turned off. This amounts to four load steps.

3.2 | Constraints

The active and reactive power sharing discrepancy of the DER as well as the node voltage and frequency deviations have to be kept within limits during steady state operation for the load cases described in Section 3.1. The active and reactive power sharing discrepancy is constrained to a maximum of 0.1 and 0.2 pu, respectively. This means that after the transients of the load steps described in Section 3.1 have decayed, the difference between the active and reactive power of the DER must be below the mentioned values. This is to ensure almost equal power sharing and to avoid overloading at steady-state.

The node voltage deviations are limited to 0.1 pu with respect to the nominal value and the frequency is allowed to differ by 500 mHz from its nominal value of 50 Hz at steady-state. These are typical constraints for LV microgrids and avoid the disconnection of loads and the tripping of under-/over-frequency relays.

The stability margin of the microgrid system is constrained by keeping the largest real part of any eigenvalue below −1 rad/s (eigenvalue real part minimisation can also be an objective as described in Section 3.3). This constraint is used when the area criterion is the objective and ensures that this stability margin is always maintained.

3.3 | Objectives

After disturbances such as load fluctuation, the DER controllers should aim at settling down to steady-state values as quickly as possible to avoid violations of component constraints and overloading. Therefore, the goal of the droop control is to minimise the area between the active/reactive power and their steady-state value. The minimisation problem is formulated as follows:

$$Min\left(\sum_{i=1}^{2}\sum_{k=1}^{4}\int_{t_{step,k}}^{t_{step,k}+t_{settle}}|p_{DER,i}(t)-p_{DER,i}(t_{step,k}+t_{settle})|+|q_{DER,i}(t)-q_{DER,i}(t_{step,k}+t_{settle})|\right), \tag{18}$$

where $i = \{1, 2\}$ is the DER number, $k = \{1, 2, 3, 4\}$ is the load step number, $p_{DER,i}(t)$ is the active power of DER i, $q_{DER,i}(t)$ is the reactive power of DER i and $t_{step,k}$ is the time of the load step k. $p/q_{DER,i}(t_{step,k} + t_{settle})$ can be seen as the steady state reference, assuming that the steady state has been reached within t_{settle} (= 4 s in this work) after a load step. These reference values are dependent on the control parameters and differ in simulations. The area to be minimised is exemplified in Figure 8. Numerical integration is applied to calculate the integrals from the time-domain simulation results.

Besides the described area criterion, the second objective used in this work is the minimisation of the largest occurring eigenvalue real part to optimise the stability of the system [39]. The decay of transients and the ability to rapidly reach a new steady-state operating point are associated with the eigenvalue real part. One of the main goals of inverter-dominated systems is to avoid transient overloading. Hence, the rapid decay of the envelope is the priority rather than other criteria, such as the damping ratio. Furthermore, extended oscillations are less of an issue in inverter-dominated networks with thoroughly optimised controller parameters as shown in Figure 10 and described in Section 5.2.

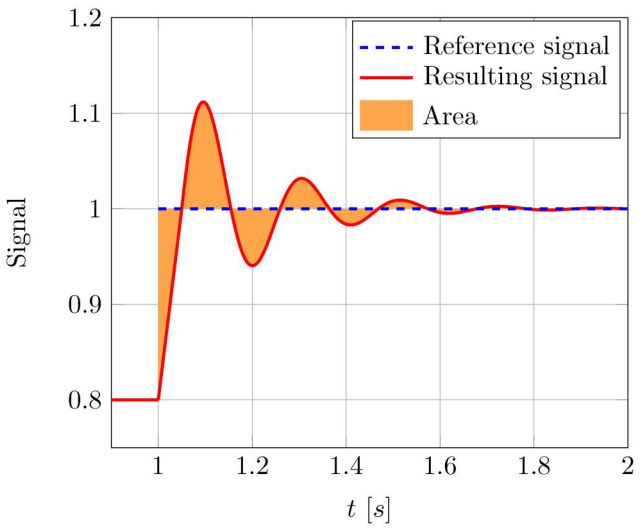

FIGURE 8 Area criterion

4 | OPTIMISATION ALGORITHM

Systematic design procedures for inverter controllers have been proposed in literature [40, 41]. However, it is either focussed on a single part of the control scheme, such as the VI [40], or the design procedure is much simplified and does not incorporate the large number of scenarios, constraints and objectives elaborated in Section 3 [41], which are necessary for a realistic assessment of the control. Furthermore, to the authors' knowledge, there is no systematic design procedure for the dynamic interaction between PED and SM (including GOV and AVR) found in literature. Hence, in this work, a heuristic method is used that can handle the intricacy of the optimisation problem, which incorporates the interaction between droop control variants, virtual impedance, AVR and GOV as well as several constraints and objectives.

GA and PSO are clearly the most common population based optimisation methods for power electronics according to a recent review [42]. A GA is a heuristic method that emulates the process of natural selection and belongs to the larger class of evolutionary algorithms. It is population based and employs the bio-inspired operators mutation, crossover and selection. The individuals in a population that are a relatively sound solution to the problem are correspondingly assigned better fitness values. This increases their chance to pass their data to the next generation [43].

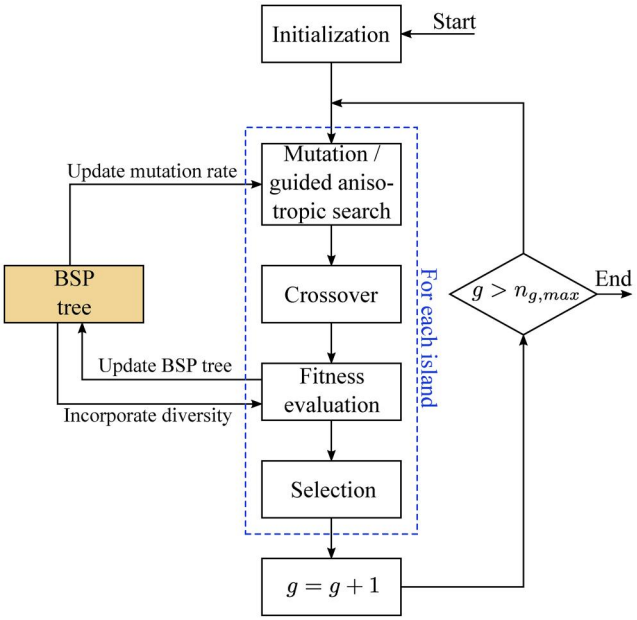

FIGURE 9 Flow chart of the enhanced GA

Here, a GA was developed that is particularly suitable for optimisation problems, where the evaluation of the fitness of the individuals comes at a high computational cost. The fitness evaluation entails the transient time domain simulation of the microgrid model, which is computationally demanding. The goal is to come to an optimal or close to optimal solution within a limited amount of fitness evaluations.

One feature is to impede the repeated evaluation of solutions that have already been evaluated in the search history of the algorithm. This incorporates the memorisation of individuals of former generations. It jointly enhances the efficiency and the diversity of the individuals. This is also referred to as a non-revisiting GA [44].

In addition to the conventional mutation, guided anisotropic search [45] is utilised. Here, former fitness values are incorporated to direct the algorithm to promising regions of the solution space. This leads to a quick convergence.

It becomes apparent that the features mentioned rely on an efficient way to save and conveniently access the data of individuals of past populations. Therefore, it is resorted to a binary space partitioning (BSP) tree [46, 47]. This method also allows the assessment of the diversity of an individual with respect to former individuals. For this purpose, the solution space is subdivided into subspaces. Each subspace represents a problem solution. The diversity of an individual is evaluated according to the size of its subspace compared to the size of the entire solution space. With the help of a diversity measure for the population, the GA can adjust its operators. For example, if the diversity becomes too low at early generations, the GA runs into the danger of premature convergence at a local optimum. The GA counteracts by increasing the likelihood of mutations. Another means to increase the diversity is to raise the fitness of diverse individuals to increase their chances in the selection.

The mentioned enhancements not only improve its efficiency, but also entail the self-adaption of the GA. By automatically controlling its diversity, it can adjust to various kinds of optimisation problems without necessarily having to tune its parameters (such as mutation rate) for each individual problem.

Niching is the idea of segmenting the population into disjoint sets, also named islands [48]. It maintains the diversity of the population and intends each island to search a different (local) optimum. It prevents the GA from premature convergence to one optimum. The islands can occasionally exchange individuals.

The flow chart of the GA is shown in Figure 9. After the initialisation of the population, the operators mutation, crossover and selection according to the fitness are executed for each island. The BSP tree is updated with the data of the individuals and the corresponding fitness values. The BSP tree assesses the diversity of each individual as well as the overall diversity of the entire population. If the GA runs into danger of premature convergence, the diversity is increased. On the one hand, individuals with a large diversity are assigned a better fitness value and the mutation rate is raised. Finally, the generation number g is incremented. When the maximum number of generations is reached, the GA stops. The main parameters of the GA are found in the Appendix.

5 | RESULTS

5.1 | Optimised parameter sets

5.1.1 | Comparison of droop variants

The resulting parameter sets for the optimisation of the three droop variants are illustrated in Table 1 for the benchmark tests described in Section 3.1. At first, optimisation is looked at with respect to the area criterion. The droop parameters have a strong impact on the controller performance. The value of $m_{\omega,PED}$ is around 0.009 pu in all cases, resulting from the frequency constraint. An exception is the two PED case of the FTD. Here, the angle γ_{PED} is at 3° which corresponds to the inverse droop. This also causes the virtual resistance $R_{vi,PED}$ to be very high and the virtual inductance $L_{vi,PED}$ to be zero as this droop type is based on a high R/X-ratio. Parameter $m_{v,PED}$ takes on relatively small values in all cases. This implies that using the VI to regulate power sharing and voltage drop is more effective. The voltage regulation by the VI is faster because the unfiltered current measurement is used to calculate the voltage drop over the VI and it directly takes effect on the output voltage setting of the voltage controller. In contrast, regulating the voltage by the voltage droop coefficient m_v is slower because this control loop requires low-pass filtering of power measurements.

The virtual inductor $L_{vi,PED}$ is usually between around 1 and 2 mH and the value of the virtual resistor $R_{vi,PED}$ is generally about 0.5 Ω for the given DER ratings. For TD and FFD, $R_{vi,PED}$ is smaller in case of two PED. As mentioned above, the VI value of the FTD for two PED is an exception.

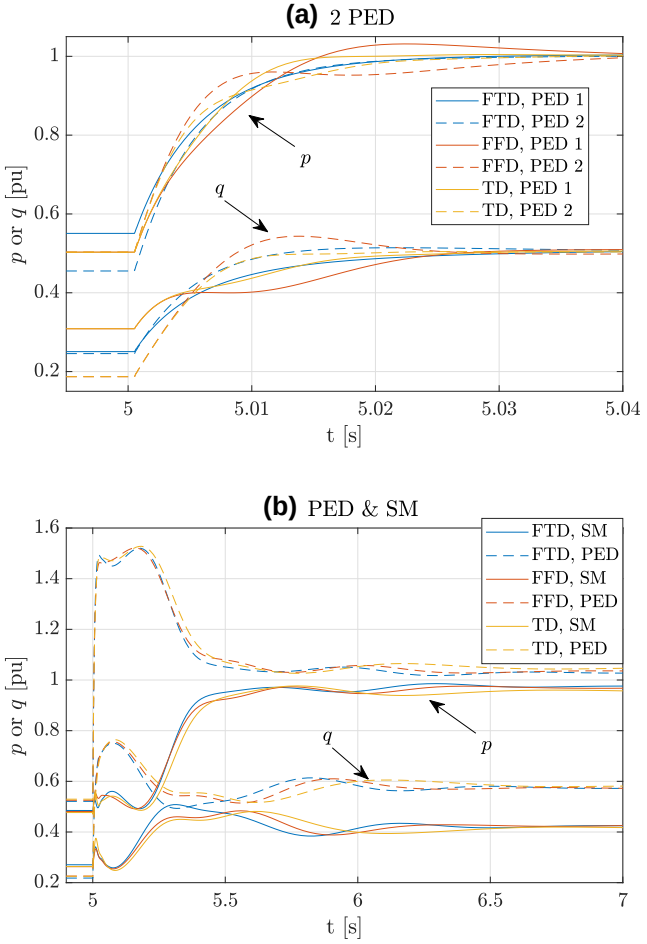

FIGURE 10 Response to load step

The transient droop coefficients $m_{\omega,t}$ and $m_{v,t,PED}$ are usually at around $0.1 \cdot 10^{-3}$ and $0.5 \cdot 10^{-3}$ pu, respectively. The feed-forward droop $m_{\omega,ff,PED}$ is the largest for the two PED case. The angle γ_{PED} of the FTD is low in case of two PED, as explained before. In the other cases, it is 90°, equivalent to the conventional droop.

The outcome for the droop coefficient $m_{\omega,SM}$ is in the same range as $m_{\omega,PED}$. $m_{v,SM}$, on the other hand, takes on much larger values than $m_{v,PED}$. Larger droop coefficients enable a quicker response of the slowly reacting SM system.

The virtual inductance of the SM $L_{vi,SM}$ is usually between 1 and 2 mH, but can also be much lower. The virtual resistor ranges between 0.24 and 0.52 Ω, which is a lower than in case of the PED.

The proportional gain of the AVR $k_{p,AVR}$ and the integral gain $k_{i,AVR}$ lie in a narrow range from 0.14 to 0.28 and from 0.18 to 0.32, respectively. The values of the proportional gain of the GOV$k_{p,GOV}$ vary between 2.8 and 6.4, whereas the integral gain $k_{i,GOV}$ exhibits only little variation.

The average area of the simulated cases is smallest for the TD, except for the case of two PED in the microgrid. Here, the ability of FTD to apply the inverse droop is advantageous. The area is considerably larger when SMs are present. Comparing the three droop types, the areas are similar for the scenarios.

For the microgrid with PED and SM, the optimised parameter sets for the minimisation of the maximum occurring eigenvalue real part are also given in Table 1. When SMs are present, the eigenvalues are closer to the unstable region and it is reasonable to optimise in terms of their minimisation. It is interesting that for both PED and SM the values for m_ω are lower compared to the area criterion optimisation. Parameter m_v is larger for the PED, whereas it decreases for the SM, where the virtual inductor $L_{vi,SM}$ increases instead. The angle γ of the FTD is at 69° for the PED, exploiting the advantages of the frame transformation. AVR and GOV are tuned less aggressively. The maximum eigenvalue real part is similar for all droop variants, although slightly increased for the FFD.

5.1.2 | Frame transformation droop

The FTD is a promising approach as it can adjust the droop control to network conditions, such as the angle of the network impedance. Therefore, a closer look is taken at each case for this droop type when optimised with respect to the area criterion. The outcome of the optimisation is depicted in Table 2. Again, a microgrid with two PED or with one PED and a SM is considered. Each case stands for a certain line length and R/X ratio.

When two PED are present, the droop coefficient $m_{\omega,PED}$ is at around 0.009 when the line length is 30 m, which is a similar value as in the optimisations in Section 5.1.1. A longer line length leads to a higher $m_{\omega,PED}$ of 0.015 pu.

Independent from the line length and R/X-ratio, $m_{v,PED}$ and $L_{vi,SM}$ are zero. The virtual resistance $R_{vi,PED}$ is highly dependent on the line length and becomes larger for longer lines. The angle γ_{PED} is low in case of two PED. The area is smaller for shorter lines and hardly depends on the R/X-ratio.

For a microgrid with one PED and one SM, the droop coefficient $m_{\omega,PED}$ takes on values around 0.009 and $m_{v,PED}$ is rather small in all cases. The virtual inductor $L_{vi,PED}$ is always below 1 mH,whereas the resistor $R_{vi,PED}$ is close to 0.5 Ω. The angle γ_{PED} is at or close to 90°.

The droop coefficient of the SM $m_{\omega,PED}$ is also at around 0.009 pu. $m_{v,SM}$ is significantly larger than $m_{v,PED}$, especially for the longer line length. The virtual inductor $L_{vi,SM}$ and resistor $R_{vi,SM}$ take on rather low values. The controller parameters of AVR and GOV are similar to those found in Section 5.1.1. The area is rather similar in all cases. Overall, the areas are slightly smaller in this Section in comparison to comparable cases in Section 5.1.1.whereas the resistor $R_{vi,PED}$ is close to 0.5 Ω. The angle γ_{PED} is at or close to 90°.

The droop coefficient of the SM $m_{\omega,PED}$ is also at around 0.009 pu. $m_{v,SM}$ is significantly larger than $m_{v,PED}$, especially for the longer line length. The virtual inductor $L_{vi,SM}$ and resistor $R_{vi,SM}$ take on rather low values. The controller

TABLE 1 Parameter sets for optimisation with respect to area criterion or eigenvalue real parts*

	TD			FFD			FTD		
	Two PED	**PED and SM**	**All cases**	**Two PED**	**PED and SM**	**All cases**	**Two PED**	**PED and SM**	**All cases**
$m_{\omega,PED}$ [pu]	0.0095	0.009/0.008*	0.0095	0.0095	0.008/0.0055*	0.009	0.015	0.008/0.0055*	0.009
$m_{v,PED}$ [pu]	0.042	0.008/0.02*	0.02	0.014	0.01/0.04*	0	0	0.016/0.042*	0.004
$L_{vi,PED}$ [mH]	1	1/0.4*	0.8	1.8	1/1*	1.8	0	0.4/0.7*	1.7
$R_{vi,PED}$ [Ω]	0.16	0.64/0.88*	0.52	0.12	0.48/0.4*	0.6	1.2	0.38/0.08*	0.56
$m_{\omega,t,PED}$[10^{-3}pu]	0.13	0.06/0.12*	0.09	–	–	–	–	–	–
$m_{v,t,PED}$ [10^{-3} pu]	0.5	0.4/0.36*	0.48	–	–	–	–	–	–
$m_{\omega,ff,PED}$ [pu]	–	–	–	0.031	0.027/0.026*	0.015	–	–	–
γ_{PED} [°]	–	–	–	–	–	–	3	90/69*	90
$m_{\omega,SM}$ [pu]	–	0.0095/0.008*	0.0095	–	0.008/0.005*	0.009	–	0.008/0.0045*	0.009
$m_{v,SM}$ [pu]	–	0.1/0.06*	0.152	–	0.124/0.076*	0.16	–	0.108/0.064*	0.148
$L_{vi,SM}$ [mH]	–	0.2/1.8*	1.8	–	1/1.4*	2	–	0/0.8*	1
$R_{vi,SM}$ [Ω]	–	0.52/0.8*	0.24	–	0.28/0.12*	0.24	–	0.24/0.16*	0.4
γ_{SM} [°]	–	84/75*	75	–	78/75*	75	–	81/84*	78
$k_{p,AVR}$ [pu]	–	0.14/0.06*	0.16	–	0.2/0.06*	0.18	–	0.28/0.08*	0.16
$k_{i,AVR}$ [pu]	–	0.18/0.12*	0.2	–	0.22/0.12*	0.22	–	0.32/0.16*	0.18
$k_{p,GOV}$ [pu]	–	2.8/2*	2.8	–	5/1.6*	6.2	–	6.4/2.6*	4.4
$k_{i,GOV}$ [pu]	–	240/260*	220	–	280/200*	280	–	300/280*	240
Average area	0.0203	1.1747	0.5920	0.0205	1.1811	0.5947	0.0199	1.1873	0.5988
Max(Re(eigenvalues))* [1/s]	–	−2.0072*	–	–	−1.9620*	–	–	−2.0009*	–

Abbreviations: FFD, feed-forward droop; FTD, frame transformation droop; PED, power electronic devices; TD, transient droop; *, optimization with respect to eigenvalue real part.

parameters of AVR and GOV are similar to those found in Section 5.1.1. The area is rather similar in all cases. Overall, the areas are slightly smaller in this Section in comparison to comparable cases in Section 5.1.1.

5.2 | Time domain simulation

The response to the connection of load 2 at $t = 5$ s is shown in Figure 10 for 2 PED and PED and SM (line length = 400 m, $R/X = 7.7$), when optimised with respect to the area criterion (parameter sets from Table 1).

In Figure 10(a), it is interesting to see that in case of the FTD, the reactive powers of the PEDs are accurately shared at steady-state ($t < 5$ s) as the frequency is a global variable, whereas the active power differs. This is a consequence of the inverse droop. FTD exhibits a very smooth, almost first-order behaviour. However, all droop variants quickly align with their steady-state value within only about two cycles.

The time-scale for PED and SM in Figure 10b is much larger due to the larger time constants of SMs. The PED is significantly overloaded following the load step, as it takes on a larger share because of its voltage source behaviour and its location at the same node as the switched load. After about 2 s, the steady state is reached. Again, the differences between the droop variants are rather small.

5.3 | Dominant eigenvalues

Figure 11 illustrates dominant eigenvalues for the cases simulated in Figure 10, except that the line length is 30 m here, which impairs the system stability. Nonetheless, the eigenvalue pairs are located very far inside the left half-plane in Figure 11a.). It becomes apparent that the eigenvalue and area criterion optimisation are not necessarily coherent, as the FTD has the largest eigenvalue real parts but performs best in power sharing. To highlight the impact of the VI, the virtual resistor $R_{vi,PED}$ is varied between 1 and 0.2 Ω (larger circles imply lower resistance) for the TD. An oscillatory mode occurs that quickly approaches the imaginary axis.

The eigenvalues of the PED and SM case are much closer to the imaginary axis. There are also oscillatory modes for all droop variants. FTD has the lowest damping ratio (16.6%) and TD has the highest (33.0%).

Besides the area criterion optimisation, the eigenvalue real part minimisation outcome is also shown. The dominant eigenvalues are at around $-2\ s^{-1}$. The damping is also improved.

TABLE 2 Parameter sets for the FTD optimisation

	2 PED			
	30 m		**400 m**	
	$R/X = 7.7$	$R/X = 3.9$	$R/X = 7.7$	$R/X = 3.9$
$m_{\omega,PED}$ (pu)	0.0085	0.009	0.015	0.015
$m_{v,PED}$ (pu)	0	0	0	0
$L_{vi,PED}$ (mH)	0	0	0	0
$R_{vi,PED}$ (Ω)	0.56	0.58	1.24	1.24
γ_{PED} (°)	9	3	3	3
Area	0.0183	0.0183	0.021	0.0211
	PED and SM			
	30 m		**400 m**	
	$R/X = 7.7$	$R/X = 3.9$	$R/X = 7.7$	$R/X = 3.9$
$m_{\omega,PED}$ (pu)	0.009	0.009	0.008	0.01
$m_{v,PED}$ (pu)	0.004	0	0.014	0
$L_{vi,PED}$ (mH)	0.5	0.4	0	0.9
$R_{vi,PED}$ (Ω)	0.52	0.36	0.4	0.64
γ_{PED} (°)	90	90	90	87
$m_{\omega,SM}$ (pu)	0.0095	0.0095	0.008	0.0095
$m_{v,SM}$ (pu)	0.072	0.044	0.104	0.144
$L_{vi,SM}$ (mH)	0	0	0	0.6
$R_{vi,SM}$ (Ω)	0.4	0.32	0.18	0.16
γ_{SM} (°)	84	84	81	84
$k_{p,AVR}$ (pu)	0.24	0.28	0.24	0.16
$k_{i,AVR}$ (pu)	0.26	0.34	0.28	0.18
$k_{p,GOV}$ (pu)	6.8	7	8	6.8
$k_{i,GOV}$ (pu)	280	280	300	260
Area	1.1026	1.1089	1.1096	1.1080

Abbreviations: FTD, frame transformation droop; PED, power electronic devices.

5.4 | Genetic algorithm

Figure 12 depicts the fitness of the best individual in the population over the generation number for the conventional and the enhanced GA according to Section 4, when optimising the FTD for the two PED scenario. The value is averaged over five runs each. The conventional GA lacks the BSP tree, the non-revisiting, the guided anisotropic search and the niching. The number of fitness function evaluations, which is a measure of the computational cost, is 700 in all cases. For comparison, also the results for the basic PSO algorithm presented in [49] are depicted.

The basic PSO algorithm performs worse than the conventional GA, what prompted this work to focus on the GA.

It becomes apparent that both GAs perform similar at early generations. Here, even the convergence to local optima results in fitness improvements. After generation four, the

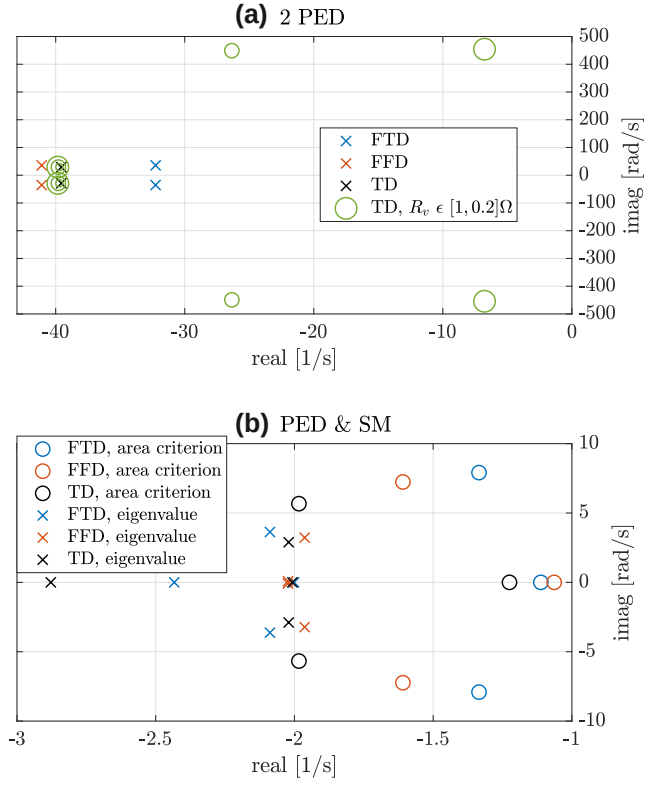

FIGURE 11 Dominant eigenvalues

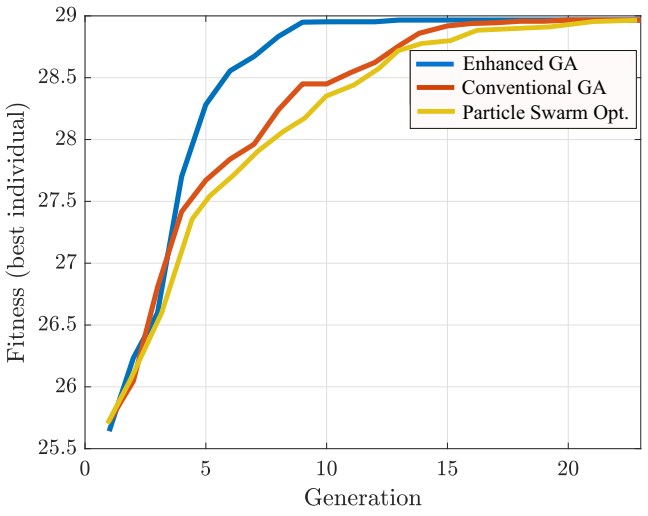

FIGURE 12 Comparison of heuristic optimisation

enhanced GA results in better fitness values. For the conventional GA, it is harder to leave local optima and search for the global optimum. Contrarily, with the help of its diversity maintaining mechanisms, the enhanced GA can improve its fitness steadily and reaches an optimal or close to optimal solution after nine generations. The conventional GA takes until generation 20 to reach the same fitness level. The slow convergence during the later generations is caused by the revisiting of similar solutions when the population has converged near the optimum.

6 | CONCLUSION AND FUTURE WORK

Three of the most popular droop variants are investigated in this work. Differences and similarities are elaborated. It is pointed out that in the previous literature the superiority of the droop variants has only been demonstrated for very specific microgrid applications which are not generally representative. To assess their performance under practical microgrid conditions, benchmark scenarios with limited simulation effort are proposed. A GA, which was tailored to problems characterised by high computational cost for the fitness evaluation, is used to optimise controller parameters and enable a fair comparison of the droop variants.

It is seen that all droop variants lead to high stability when their parameters are thoroughly optimised. The FTD has some advantages due to its flexibility and is shown to be beneficial also for SMs. However, it is demonstrated that the impact of VI on stability and power sharing is much more pronounced than the choice of the droop variant. In some scenarios, the voltage control is taken over completely by the VI, due to its fast response, and the voltage droop coefficient m_v becomes zero after optimisation.

In conclusion, the superiority of one droop variant over the others, as indicated in literature for some specific microgrid scenarios, cannot be transferred to the practical benchmark microgrid applications analysed in this work. It is rather that the thorough controller parameter optimisation and the combination with VI are distinctly more important than the choice of the droop variant.

The obtained parameter sets can be used as a basis for stability analysis of microgrids in many contexts, such as reconfiguration or topology optimisation. In future, the benchmark scenarios may be extended for harmonic analysis, more accurate dynamic load models and more complex topologies. For the latter, the efficient simulation and optimisation of larger microgrids is key. An interesting candidate here is the upcoming highly efficient Julia programming language, where some open-source toolboxes for power system simulation are already available [50]. Furthermore, only three of the most popular controller types were considered in this work and further variants should be included in future.

ACKNOWLEDGEMENT

Open Access funding enabled and organized by Projekt DEAL.

ORCID

Simon Eberlein https://orcid.org/0000-0001-6951-2811
Krzysztof Rudion https://orcid.org/0000-0003-0929-2479

REFERENCES

1. Hatziargyriou, N.: Microgrids: Architectures and Control. Wiley-IEEE Press, Chichester, West Sussex (2014). oCLC: 1087331705
2. Vandoorn, T.L., et al.: Review of primary control strategies for islanded microgrids with power-electronic interfaces. Renew Sustain. Energy Rev. 19, 613–628 (2013). http://www.sciencedirect.com/science/article/pii/S1364032112006764
3. Han, H., et al.: Review of power sharing control strategies for islanding operation of AC microgrids. IEEE Trans. Smart Grid. 7(1), 200–215 (2016)
4. He, J., Li, Y.W.: An enhanced microgrid load Demand sharing strategy. IEEE Trans. Power Electron. 27(9), 3984–3995 (2012)
5. Vasquez, J.C., et al.: Adaptive droop control applied to voltage-source inverters operating in grid-connected and islanded modes. IEEE Trans. Ind. Electron. 56(10), 4088–4096 (2009)
6. Li, Y.W., Kao, C.: An accurate power control strategy for power-electronics-Interfaced distributed generation units operating in a low-voltage multibus microgrid. IEEE Trans. Power Electron. 24(12), 2977–2988 (2009)
7. Mohamed, Y., El-Saadany, E.F.: Adaptive decentralized droop controller to preserve power sharing stability of parallelled inverters in distributed generation microgrids. IEEE Trans Power Electron. 23(6), 2806–2816 (2008)
8. Engler, A.: Regelung von Batteriestromrichtern in modularen und erweiterbaren Inselnetzen. (PhD dissertation). University of Kassel. Kassel (2002)
9. Brabandere, K.D., et al.: A voltage and frequency droop control method for parallel inverters. IEEE Trans. Power Electron. 22(4), 1107–1115 (2007)
10. Wu, T., et al.: A unified virtual power decoupling method for droop-controlled parallel inverters in microgrids. IEEE Trans. Power Electron. 31(8), 5587–5603 (2016)
11. Li, P., et al.: Dynamic power conditioning method of microgrid via adaptive inverse control. IEEE Trans. Power Deliv. 30(2), 906–913 (2015)
12. Li, Y., Li, Y. W.: Power management of inverter interfaced autonomous microgrid based on virtual frequency-voltage frame. IEEE Trans. Smart Grid. 2(1), 30–40 (2011)
13. Guerrero, J.M., et al.: Decentralized control for parallel operation of distributed generation inverters using resistive output impedance. IEEE Trans. Ind. Electron. 54(2), 994–1004 (2007)
14. Wai, R.-J., Zhang, Q.-Q., Wang, Y.: A novel voltage stabilisation and power sharing control method based on virtual complex impedance for an off-grid microgrid. IEEE Trans. Power Electron. 34(2), 1863–1880 (2019)
15. Hu, J., et al.: Virtual flux droop method-A new control strategy of inverters in microgrids. IEEE Trans Power Electron. 29(9), 4704–4711 (2014)
16. Zhang, Y., Xie, L., Ding, Q.: Interactive control of coupled microgrids for guaranteed system-wide small signal stability. IEEE Trans. Smart Grid. 7(2), 1088–1096 (2016)
17. Trivedi, A., Jain, D.K., Singh, M.: A modified droop control method for parallel operation of VSI's in microgrid. In: IEEE Innovative Smart Grid Technologies-Asia (ISGT Asia), pp. 1–5. Bangalore (2013)
18. Simpson-Porco, J.W., Doerfler, F., Bullo, F.: Voltage stabilisation in microgrids via quadratic droop control. IEEE Trans. Automat. Contr. 62(3), 1239–1253 (2017)
19. Elrayyah, A., Cingoz, F., Sozer, Y.: Construction of nonlinear droop relations to optimise islanded microgrid operation. IEEE Trans. Ind. Appl. 51(4), 3404–3413 (2015)
20. Dou, C., et al.: Improved droop control based on virtual impedance and virtual power source in low-voltage microgrid. IET Gener., Transm. Distrib. 11(4), 1046–1054 (2017)
21. Peng, Z., et al.: The application of microgrids based on droop control with coupling compensation and inertia. IEEE Trans. Sustain. Energy. 9(3), 1157–1168 (2018)
22. Wu, X., Shen, C., Iravani, R.: Feasible range and optimal value of the virtual impedance for droop-based control of microgrids. IEEE Trans. Smart Grid. 8(3), 1242–1251 (2017)
23. Yu, K., et al.: Analysis and optimization of droop controller for microgrid system based on small-signal dynamic model. IEEE Trans. Smart Grid. 7(2), 695–705 (2016)
24. Dheer, D.K., et al.: Effect of placement of droop based generators in distribution network on small signal stability margin and network loss. Intl. J. Electr. Power Energy Syst. 88, 108–118 (2017)
25. Dheer, D.K., et al.: Effect of reconfiguration and Meshed networks on the small-signal stability margin of droop-based islanded microgrids. IEEE Trans. Ind. Appl. 54(3), 2821–2833 (2018)
26. Eberlein, S., Rudion, K.: Small-signal stability modelling, sensitivity analysis and optimization of droop controlled inverters in LV microgrids. Intl. J. Electr. Power Energy Syst. 125, 106404 (2021)

27. Pogaku, N., Prodanovic, M., Green, T.C.: Modeling, analysis and testing of autonomous operation of an inverter-based microgrid. IEEE Trans. Power Electron. 22(2), 613–625 (2007)
28. Bacha, S., Munteanu, I., Bratcu, A.I.: Power electronic converters modelling and control. In: Grimble, M.J., Johnson, M.A. (eds.) Advanced Textbooks in Control and Signal Processing. Springer London, London (2014)
29. Eberlein, S., Heider, A., Rudion, K.: Modelling and control optimization of diesel synchronous generators in LV microgrids. In: 2018 IEEE PES Innovative Smart Grid Technologies Conference Europe (ISGT-Europe), pp. 1–6. Sarajevo (2018)
30. Krause, P.C., et al.: Analysis of electric machinery and drive systems. In: IEEE Press series on power engineeering, 3rd ed. Wiley, Hoboken, (2013)
31. Paquette, A.D.: Power quality and inverter-generator interactions in microgrids. [PhD dissertation]. Georgia Institute of Technology, Atlanta, Georgia (2014)
32. Gkountaras, A.: Modeling Techniques and Control Strategies for Inverter Dominated Microgrids, vol. 2. Universitaetsverlag der TU Berlin, Berlin (2017)
33. Chandorkar, M.C., Divan, D.M., Adapa, R.: Control of parallel connected inverters in standalone AC supply systems. IEEE Trans. Ind. Appl. 29(1), 136–143 (1993)
34. Canizares, C., et al.: Benchmark models for the analysis and control of small-signal oscillatory dynamics in power systems. IEEE Trans. Power Syst. 32(1), 715–722 (2017)
35. Ayaz, M.S., Azizipanah Abarghooee, R., Terzija, V.: European LV microgrid benchmark network: development and frequency response analysis. In: 2018 IEEE international energy conference (ENERGYCON). pp. 1–6. Limassol, Cyprus (2018)
36. Pulcherio, M.C., Illindala, M.S., Yedavalli, R.K.: Robust stability region of a microgrid under parametric uncertainty using bialternate sum matrix approach. IEEE Trans. Power Syst. 33(5), 5553–5562 (2018)
37. Krismanto, A.U., Mithulananthan, N., Kamwa, I.: Oscillatory stability assessment of microgrid in autonomous operation with uncertainties. IET Renew. Power Gener. 12(4), 494–504 (2018)
38. Baimel, D., et al.: Dynamic modeling of networks, microgrids, and renewable sources in the dq0 reference frame: a Survey. IEEE Access. 5, 21323–21335 (2017)
39. Hassan, M.A., Abido, M.A.: Optimal design of microgrids in autonomous and grid-connected modes using particle swarm optimization. IEEE Trans. Power Electron. 26(3), 755–769 (2011)
40. He, J., Li, Y.W.: Analysis, design, and implementation of virtual impedance for power electronics Interfaced distributed generation. IEEE Trans. Ind. Appl. 47(6), 2525–2538 (2011)
41. Cabero Rodriguez, A., Roldan.Perez, J., Prodanovic, M.: Virtual impedance design considerations for virtual synchronous machines in weak grids. IEEE Trans. Emerg. Sel. Topics Power Electron. 8(2), 1477–1489 (2019)
42. Zhao, S., Blaabjerg, F., Wang, H.: conference Name.An overview of artificial intelligence applications for power electronics, IEEE Trans Power Electron. vol. 36(4), pp. 4633–4658 (2021)
43. Lee, K.Y., et al., IEEE Press: Modern heuristic optimization techniques: theory and applications to power systems. Wiley-Interscience, Piscataway, NJ (2008)
44. Yuen, S.Y., Chow, C.K.: A genetic algorithm that Adaptively Mutates and Never Revisits. IEEE Trans. Evol. Comput. 13(2), 454–472 (2009)
45. Chow, C.K., Yuen, S.Y.: An evolutionary algorithm that makes decision based on the entire previous search history. IEEE Trans. Evol. Comput. 15(6), 741–769 (2011)
46. Hearn, D., Baker, M.P., Carithers, W.R. (eds.): Computer Graphics with OpenGL, 4th ed. Pearson, Harlow (2014)
47. Berg, M.d., et al.: Computational Geometry: Algorithms and Applications, 3rd ed. Springer, Berlin (2008)
48. Zhu, J.: Optimization of power system operation. In: IEEE Press series on power engineering. Wiley-IEEE, Chichester (2009). Piscataway
49. Radloff, M.: Evolutionary Algorithm for Optimization Compute-Intensive Fitness Functions. University of Stuttgart, Stuttgart (2019)
50. Henriquez Auba, R., et al.: LITS.jl – an open-source Julia based simulation Toolbox for low-inertia power systems: arXiv 200302957 [cs, eess, math]. (2020). arXiv: 2003.02957 http://arxiv.org/abs/2003.02957

How to cite this article: Eberlein, S., Rudion, K.: Optimisation, benchmark testing and comparison of droop control variants in microgrids. IET Smart Grid. 4(5), 536–548 (2021). https://doi.org/10.1049/stg2.12036

APPENDIX

Grid-forming PED [26]: $V_n = 400$ V, $S_n = 10$ kVA, $\omega_c = 60$, $v_0 = 1, f_0 = 1, k_{p,v} = 3, k_{i,v} = 200, FF_v = 1, k_{p,c} = 0.73, k_{i,c} = 50$, $FF_c = 1, L_1 = 1.5$ mH, $R_1 = 0.1\ \Omega$, $C_f = 70\ \mu F, L_2 = 0.36$ mH.

SM [29]: $S_n = 10$ kVA, $V_n = 400$ V, $x_{ls} = 0.064$ pu, $x_{md} = 1.65$ pu, $x_{lkq1} = 0.41$ pu, $x_{mq} = 1.159$ pu, $x_{lkq2} = 0$ pu, $x_{lfd} = 0.468$ pu, $x_{lkd} = 0.07$ pu, $r_s = 0.062$ pu, $r_{rkq1} = 0.111$ pu, $r_{kq2} = 0$ pu, $r_{fd} = 0.0674$ pu, $r_{kd} = 0.147$ pu.

AVR [29]: $K_A = 400$, $T_A = 0.2$ s, $T_E = 0.8$ s, $K_E = 1$, $e_{xfd,1} = 5.6$, $E_{xfd,2} = 4.4$, $s_{Efd,1} = 0.86$, $s_{Efd,2} = 0.5$, $T_r = 0.02$.

GOV [29]: $T_1 = 0.07$ s, $T_2 = 0.125$ s, $K_1 = 1.15$, $K_2 = 1$, $K_3 = 1$.